

Effects of nucleon-nucleon short-range correlation on fragment generation in isotopic nuclear reactions*

Ya-Fei Guo (郭亚飞)¹ Yong-Qing Feng (冯永清)¹ Zhao-Qing Feng (冯兆庆)² Gao-Chan Yong (雍高产)^{3,4}
Chun-Wang Ma (马春旺)^{1,5†}

¹College of Physics, Centre for Theoretical Physics, Henan Normal University, Xinxiang 453007, China

²School of Physics and Optoelectronics, South China University of Technology, Guangzhou 510641, China

³Institute of Modern Physics, Chinese Academy of Sciences, Lanzhou 730000, China

⁴School of Nuclear Science and Technology, University of Chinese Academy of Sciences, Beijing 100049, China

⁵Institute of Nuclear Science and Technology, Henan Academy of Sciences, Zhengzhou, 450046, China

Abstract: The effects of nucleon-nucleon short-range correlations lead to the high-momentum tail (HMT) in the nucleon momentum distribution, is displayed by the isospin- and momentum-dependent Lanzhou quantum molecular dynamics (LQMD) transport model. Based on the transport model, we studied the effects of the HMT of nucleon momentum distribution in initialization in isotopic nuclear reactions at a beam energy of 120 MeV/u. The single and double ratios of gas-phase neutron and proton spectra are analyzed and compared with experimental data in central $^{112}\text{Sn}+^{112}\text{Sn}$ and $^{124}\text{Sn}+^{124}\text{Sn}$ collisions. The HMT affects the single ratios but not the double ratios that can be employed to study other isospin effects more effectively. The ratio of triton and ^3He of light clusters contained in the gas-phase nucleons is certainly also influenced by HMT. Combining with the QMD transport model that can describe multi-fragmentation and the production of fragments in intermediate-energy heavy-ion collisions, we have studied the short-range correlation effect on fragments generation. It is found that the isospin-dependent high-momentum tail evidently affects the fragment multiplicity distribution and the average neutron to proton ratio of produced isobars.

Keywords: nucleon-nucleon short-range correlation, high-momentum tail, nuclear fragmentation reaction, LQMD transport model

DOI: CSTR:

I. INTRODUCTION

The saturation character of nuclear matter reveals a balance between long-range attractive forces and short-range repulsive forces within the nuclear interaction. This short-range aspect of nuclear forces engenders correlations among nucleon pairs, especially neutron-proton ($n-p$) pairs, which give rise to nucleons in the ground state populating the phase space with momenta exceeding the Fermi momentum [1–5]. The high-momentum tail (HMT) phenomenon, resulting from nucleon-nucleon short-range correlations (SRCs), has been substantiated through proton removal experiments using high-energy electrons or protons [6–11]. Recent experiments with high momentum transfer indicate that nuclei in the ground state can form nucleon pairs characterized by high relative momentum and low center-of-mass momentum [12–16]. Such findings reveal that approximately 20% of

nucleons in the ground state exist in these paired states, focusing interest on these intricate nucleon correlations [17–21]. Furthermore, the HMT profile typically exhibits a C/k^4 tail across all nuclei, ranging from deuterons to much heavier nuclei [22–25]. In the nucleon momentum distribution within the HMT, the ratio of $n-p$ SRC to $p-p$ or $n-n$ SRC is approximately 18 in heavier nuclei [26, 27], but significantly lower in lighter nuclei ($A < 5$) [28]. Consequently, the nucleon component in the HMT is markedly isospin dependent, indicating distinct structures in the high-momentum wave function, particularly in lighter nuclei.

Using the isospin- and momentum-dependent transport model, one can study the isospin effect in intermediate-energy heavy-ion collisions (HICs) through some isospin-sensitive observables, such as nucleonic collective flows, the free neutron to proton ratio (n/p), and the π^-/π^+ ratio [29–32]. They all have been shown to be

Received 1 April 2025; Accepted 14 May 2025

* This work is supported by the National Natural Science Foundation of China (No. 12305130), China Postdoctoral Science Foundation (No. 2023M731016), Henan Postdoctoral Foundation (No. HN2022164) and the Natural Science Foundation of Henan Province (No. 242300422048)

† E-mail: machunwang@126.com

©2025 Chinese Physical Society and the Institute of High Energy Physics of the Chinese Academy of Sciences and the Institute of Modern Physics of the Chinese Academy of Sciences and IOP Publishing Ltd. All rights, including for text and data mining, AI training, and similar technologies, are reserved.

more or less sensitive to the HMT [33–35]. And the quantum molecular dynamics transport model can better explain the multi-fragmentation and the production of fragments in intermediate-energy HICs [36–38]. Since the effects of nucleon-nucleon SRC on fragments and the light clusters, e.g., triton and ^3He are studied with central $^{112}\text{Sn} + ^{112}\text{Sn}$ and $^{124}\text{Sn} + ^{124}\text{Sn}$ collisions at $E_{\text{beam}} = 120$ MeV/u. Before this work, we first constructed the HMT of the initializing nucleus in phase space. Afterwards, the gas-phase nucleons sensitive to the high-momentum tail is studied in the transport model with the HMT of the initializing nucleus, and compared with experimental data. Simultaneously, as a verification of the constructed HMT, it offers certain evidentiary support for the subsequent study of fragments and the light clusters.

II. QMD MODEL WITH THE HMT INITIALIZATION

In the QMD-like models, the wave function for each nucleon is represented by Gaussian wave packet [39, 40] as follows

$$\psi_i(\mathbf{r}, t) = \frac{1}{(2\pi\sigma_r^2)^{3/4}} \exp\left[-\frac{[\mathbf{r} - \mathbf{r}_i(t)]^2}{4\sigma_r^2}\right] \exp\left(\frac{i\mathbf{p}_i(t) \cdot \mathbf{r}}{\hbar}\right), \quad (1)$$

where $\mathbf{r}_i(t)$ and $\mathbf{p}_i(t)$ are the centers of the i^{th} nucleon in the coordinate and momentum space, respectively. σ_r is the width of the Gaussian wave packet depending on the mass number of the nucleus in $\sigma_r = 0.92 + 0.08A^{1/3}$ fm [41]. After performing a Wigner transformation for Eq. (1), the Wigner density is obtained as,

$$f(\mathbf{r}, \mathbf{p}, t) = \sum_i f_i(\mathbf{r}, \mathbf{p}, t), \quad (2)$$

with

$$f_i(\mathbf{r}, \mathbf{p}, t) = \frac{1}{(\pi\hbar)^3} \exp\left[-\frac{[\mathbf{r} - \mathbf{r}_i(t)]^2}{2\sigma_r^2} - \frac{[\mathbf{p} - \mathbf{p}_i(t)]^2}{2\sigma_p^2}\right]. \quad (3)$$

The i^{th} nucleon density distribution in the coordinate and momentum space are

$$\rho_i(\mathbf{r}, t) = \frac{1}{(2\pi\sigma_r^2)^{3/2}} \exp\left[-\frac{[\mathbf{r} - \mathbf{r}_i(t)]^2}{2\sigma_r^2}\right] \quad (4)$$

and

$$g_i(\mathbf{p}, t) = \frac{1}{(2\pi\sigma_p^2)^{3/2}} \exp\left[-\frac{(\mathbf{p} - \mathbf{p}_i(t))^2}{2\sigma_p^2}\right], \quad (5)$$

respectively, and the total density distributions are the

sum of all nucleons in reaction systems.

In the LQMD model, the temporal evolutions of the baryons (nucleons and resonances) and mesons in the reaction system under the self-consistently generated mean-field are governed by Hamilton's equations of motion [42–46]. On the basis of the Skyrme interactions, isospin-, density-, and momentum-dependent Hamiltonians were constructed. The Hamiltonian of baryons consists of the relativistic energy, effective interaction potential, and momentum related components. The effective interaction potential is composed of the Coulomb potential and the local interactions.

The local interaction potential is derived from the energy-density functional in the form $U_{\text{loc}} = \int V_{\text{loc}}(\rho(\mathbf{r}))d\mathbf{r}$. The functional $\int V_{\text{loc}}$ can be written as:

$$V_{\text{loc}}(\rho) = \frac{\alpha}{2} \frac{\rho^2}{\rho_0} + \frac{\beta}{1+\gamma} \frac{\rho^{1+\gamma}}{\rho_0^\gamma} + E_{\text{sym}}^{\text{loc}}(\rho)\rho\delta^2 + \frac{g_{\text{sur}}}{2\rho_0} (\nabla\rho)^2 + \frac{g_{\text{sur}}^{\text{iso}}}{2\rho_0} [\nabla(\rho_n - \rho_p)]^2, \quad (6)$$

where ρ_n , ρ_p and $\rho = \rho_n + \rho_p$ are the neutron, proton, and total densities, respectively, and $\delta = (\rho_n - \rho_p)/(\rho_n + \rho_p)$ is the isospin asymmetry. The parameters α , β , γ , g_{sur} , $g_{\text{sur}}^{\text{iso}}$ and ρ_0 are set to -215.7 MeV, 142.4 MeV, 1.322 MeV fm 2 , -2.7 MeV fm 2 , and 0.16 fm $^{-3}$, respectively. $E_{\text{sym}}^{\text{loc}}(\rho) = 26.25(\rho/\rho_0)^{0.5}$ is the local part of the symmetry energy, which leads to soft-symmetry energy and the effective mass splitting of $m_n^* > m_p^*$ to obtain the symmetry energy of 31.5 MeV at saturation density. In the LQMD model, a Skyrme-type momentum-dependent potential is used [42, 43].

$$U_{\text{mom}} = \frac{1}{2\rho_0} \sum_{i,j,j \neq i} \sum_{\tau,\tau'} C_{\tau,\tau'} \delta_{\tau,\tau} \delta_{\tau',\tau_j} \int \int \int d\mathbf{p} d\mathbf{p}' d\mathbf{r} \times f_i(\mathbf{r}, \mathbf{p}, t) [\ln(\epsilon(\mathbf{p} - \mathbf{p}')^2 + 1)]^2 f_j(\mathbf{r}, \mathbf{p}', t), \quad (7)$$

in which $C_{\tau,\tau} = C_{\text{mom}}(1+x)$, $C_{\tau,\tau'} = C_{\text{mom}}(1-x)$ ($\tau \neq \tau'$) and the isospin symbols $\tau(\tau')$ represent the proton or neutron. The parameters C_{mom} and ϵ were determined by fitting the real part of the optical potential as a function of the incident energy from the proton-nucleus elastic scattering data, and the obtained values of C_{mom} and ϵ were 1.76 MeV and 500 c 2 /GeV 2 , respectively. Thus, the effective mass of the nuclear medium at saturation density is $m^*/m = 0.75$. The parameter x is the strength of the isospin splitting, for which a value of -0.65 is adopted in this study, and the mass splitting is $m_n^* > m_p^*$ in the nuclear medium [47].

The initial density distributions of nucleons in the projectile and target come from the density distributions of stable nuclei selected by the self-evolution of nucleons

in the LQMD model. Each nucleus is divided into many spherical shells centered around its center of mass. By using the local Thomas-Fermi approximation in each shell of radius r , the local Fermi momenta of neutrons and the protons in each shell are calculated according to

$$k_{F_{n,p}}^*(r) = [3\pi^2 \rho(r)_{n,p}]^{1/3}, \quad (8)$$

where $\rho(r)$ is given by Eq. (4). The Fermi momentum obtained based on Eq. (8) can provide nuclear momentum space information by using the Monte Carlo sampling method.

We use a nucleon momentum distribution with a high-momentum tail reaching $\lambda k_{F_{n,p}} = 2.0 k_{F_{n,p}}$ [48], where $\lambda = k_{max}/k_F$ is the high momentum cutoff parameter and $k_{F_{n,p}}$ is the neutron or proton Fermi momentum [49, 50]. According to the n - p dominance model [26, 27], 20% of nucleons with equal numbers of neutrons and protons are inside the HMT. The momentum distribution for nucleons with high-momentum tail in initialization reads

$$n^{HMT}(k) \propto 1/k^4 \quad (9)$$

and

$$n(k) = \begin{cases} C_1, & k \leq k_F; \\ C_2/k^4, & k_F < k < \lambda k_F, \end{cases} \quad (10)$$

keeping 20% fraction of total nucleons in the HMT, i.e.,

$$\int_{k_F}^{\lambda k_F} n^{HMT}(k) k^2 dk / \int_0^{\lambda k_F} n(k) k^2 dk = 20\% \quad (11)$$

with the normalization condition

$$\int_0^{\lambda k_F} n(k) k^2 dk = 1. \quad (12)$$

In the above equations, the parameters C_1 and C_2 in Eq. (10) are determined automatically from the above equations. The calculation of momentum distribution also uses the form of Gaussian wave packet in Eq. (5).

The HMT is strongly isospin dependent and the isotopes ^{112}Sn and ^{124}Sn have been applied to the study of isospin effects. Therefore, the HMT of ^{112}Sn and ^{124}Sn have been constructed as shown in Fig. 1. The nucleon momentum distributions with and without HMT are compared. Compared to the ideal gas case, protons in the neutron-rich nucleus ^{124}Sn have a higher probability than neutrons of possessing momenta exceeding the nuclear without HMT momentum [51]. This phenomenon arises from the n - p dominance model, which dictates that equal

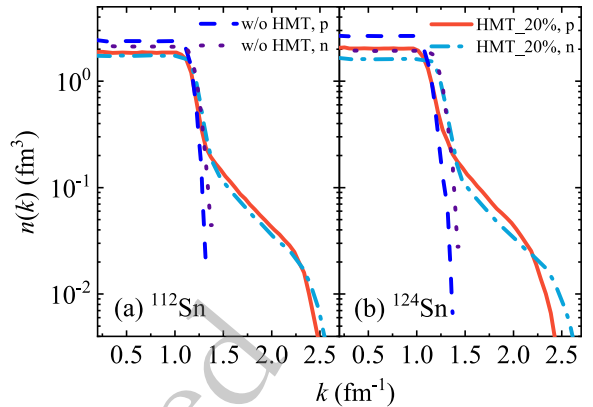


Fig. 1. (Color online) Comparison between nucleon momentum distribution $n(k)$ of ^{112}Sn and ^{124}Sn with and without HMT. The normalization condition $\int_0^{\lambda k_F} n(k) k^2 dk = 1$.

numbers of neutrons and protons must populate the HMT.

III. RESULTS AND DISCUSSION

Since the performance of nucleons is relevant to the isospin-dependent HMT, the observables should be kinetic-energy spectra or momentum spectra with isospin correlation. The central collisions of the isotopic nuclear systems $A = ^{112}\text{Sn} + ^{112}\text{Sn}$ and $B = ^{124}\text{Sn} + ^{124}\text{Sn}$ are simulated at $E_{beam} = 120$ MeV/u and an impact parameter $b = 0 - 3$ fm to investigate the effects of the HMT on the kinetic-energy spectra of neutron-to-proton ratios ($R_{n/p}$) from the yields of gas-phase fragments (nucleons, hydrogen and helium isotopes) in Fig. 2. These particles, emitted perpendicular to the beam direction with a cut at the polar angle of $70^\circ < \theta_{c.m.} < 110^\circ$ ($\cos \theta_{c.m.} = p_z / \sqrt{p_x^2 + p_y^2 + p_z^2}$), are analyzed. The nucleons in the gas phase of the experimental data are obtained by combining the free nucleons with those bound in light isotopes with $1 < A < 5$ [52, 53]. As shown in Fig. 2, it can be observed that the value of the gas-phase $R_{n/p}$ without the HMT is obviously higher than that with the HMT, both in $^{112}\text{Sn} + ^{112}\text{Sn}$ and $^{124}\text{Sn} + ^{124}\text{Sn}$ collisions. The HMT is induced by SRCs and the n - p pairs are predominant. This predominance implies that in the high-kinetic energy region, neutrons and protons are more prone to appear as correlated pairs, resulting in reduced $R_{n/p}$. The reduction in the n/p ratio will tend to approach 1, and the extent of the reduction will become smaller as the isospin asymmetry of the reaction system decreases. Therefore, the HMT effect in neutron-rich reaction systems is more noticeable. It can also be seen that in both $^{112}\text{Sn} + ^{112}\text{Sn}$ and $^{124}\text{Sn} + ^{124}\text{Sn}$ collisions under the influence of soft symmetry energy and the effective mass splitting of $m_n^* > m_p^*$, the gas-phase $R_{n/p}$ with the HMT is closer to the experimental data than that without the HMT. On the other

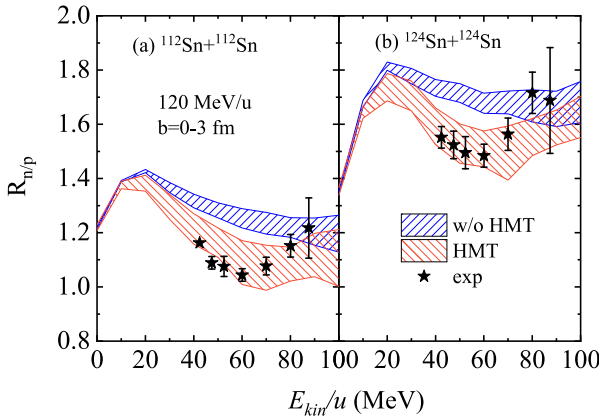


Fig. 2. (Color online) Effects of the HMT on the kinetic-energy spectra of neutron to proton ratios from the yields of gas-phase fragments (nucleons, hydrogen and helium isotopes) [panels (a) and (b)] in $^{112}\text{Sn} + ^{112}\text{Sn}$ and $^{124}\text{Sn} + ^{124}\text{Sn}$ reactions at the beam energy $E_{\text{beam}} = 120 \text{ MeV/u}$ in the transverse direction $70^\circ < \theta_{\text{c.m.}} < 110^\circ$.

hand, the bump structure around the energy of 20 MeV/u comes from the competition of free nucleons and light fragments to $R_{n/p}$. The light fragments with $Z \leq 2$ are mainly produced at low kinetic energy and have smaller n/p ratios in comparison to the free nucleons [44].

The kinetic energy spectra of the gas-phase double neutron-to-proton ratios ($DR_{n/p} = R_{n/p}(B)/R_{n/p}(A)$) has been calculated at $E_{\text{beam}} = 120 \text{ MeV/u}$ in the transverse direction $70^\circ < \theta_{\text{c.m.}} < 110^\circ$ with and without the HMT as shown in Fig. 3. However, the $DR_{n/p}$ whether with or without the HMT is less sensitive to the experimental data since the HMT has the same effect on neutron-rich and -deficient systems. Therefore, the $DR_{n/p}$ serves as a good experimental observable for other isospin effects, such as symmetry energy and nucleon effective mass splitting, because it can be considered without taking into account the HMT, neutron measurement efficiency, and the influence of Coulomb energy.

Among gas-phase nucleons, light clusters such as triton and ^3He constitute essential components. Therefore, analyzing the triton-to- ^3He ratio enables us to further explore the isospin-dependent effects within gas-phase nucleons and establish an understanding of the dynamics of light clusters under the influence of HMT. Shown in Fig. 4 is the triton-to- ^3He ratio as a function of the total momentum in the peripheral collisions of 120 MeV/u $^{112}\text{Sn} + ^{112}\text{Sn}$ and $^{124}\text{Sn} + ^{124}\text{Sn}$. With respect to HMT, it is seen that the triton-to- ^3He ratio is sensitive to HMT. Moreover, the value of the triton-to- ^3He ratio with HMT is much smaller than that without HMT, especially at high momenta. This is due to the fact that the HMT arises from SRCs, where $n-p$ pairs dominate. This dominance suggests that neutrons and protons in the high-momentum region are more likely to form correlated pairs,

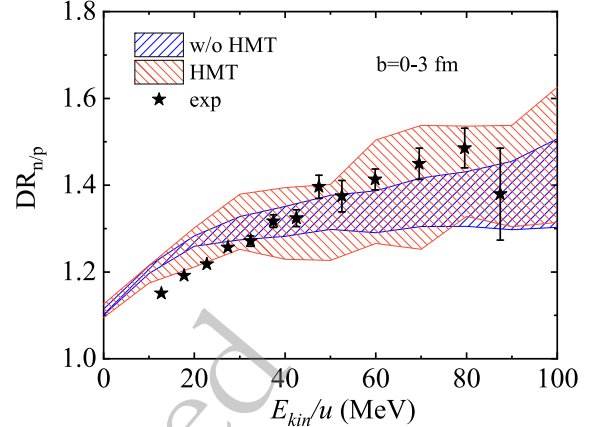


Fig. 3. (Color online) Effects of the HMT on the kinetic-energy spectra of the double neutron to proton ratios of gas-phase nucleons in collisions of $^{124}\text{Sn} + ^{124}\text{Sn}$ over $^{112}\text{Sn} + ^{112}\text{Sn}$ at the beam energy $E_{\text{beam}} = 120 \text{ MeV/u}$ in the transverse direction $70^\circ < \theta_{\text{c.m.}} < 110^\circ$.

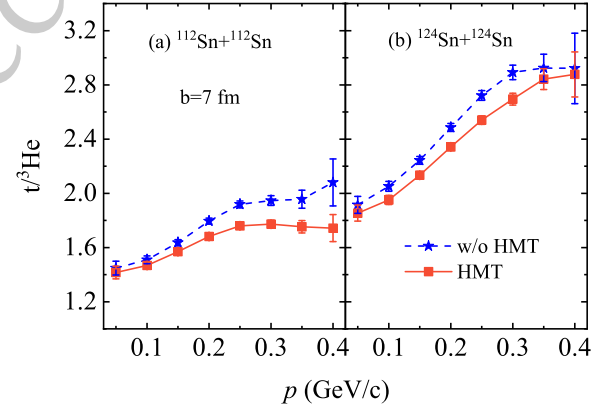


Fig. 4. (Color online) Effects of the HMT on the triton to ^3He ratio as a function of total momentum in the Sn+Sn reactions at 120 MeV/u with different reaction systems.

leading to a decrease in the triton-to- ^3He ratio. For the peripheral collisions, since more (less) energetic nucleons are from the HMT (nucleon-nucleon collisions), the larger effects of the HMT on the triton-to- ^3He ratio are expected.

Light clusters, such as triton and ^3He , offer insights into isospin dynamics under the influence of the HMT. Extending this analysis, it turns to heavier fragments whose production involves more complex interactions and structural dynamics. Figure 5 shows multiplicity distributions of fragments produced in HICs with and without HMT in the peripheral collisions of $^{112}\text{Sn} + ^{112}\text{Sn}$ and $^{124}\text{Sn} + ^{124}\text{Sn}$. It can be seen that the yields of fragments decrease with the increasing fragment charge whether with or without the HMT and are not affected by the different isotope reaction systems. However, it is clear that there are more yields of very light fragments and less yields of heavier fragments with the HMT com-

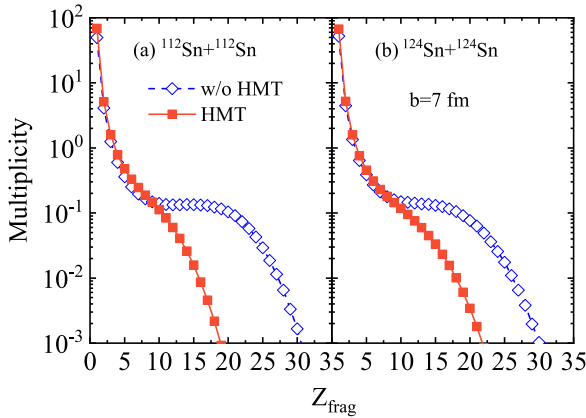


Fig. 5. (Color online) Effects of the HMT on the multiplicities of fragments as a function of fragment charge in the Sn+Sn reactions at 120 MeV/u with different reaction systems.

pared to without the HMT. This is because the very light fragments are mostly pre-equilibrium emissions, the momentum correlations among nucleons increase the coalescence probability among nucleons, thus more light fragments are produced. The heavier fragments are mainly deexcited remnants of the reaction, thus, heavier fragments are produced with smaller nucleon momenta (i.e., without the HMT).

Due to the dominant isospin dependence of short-range correlation pairs, in addition to the multiplicity distribution, the influence of the HMT should also be reflected in average neutron to proton ratio $\langle N/Z \rangle$ of the fragments. Figure 6 shows the $\langle N/Z \rangle$ as a function of the fragment charge number A_{frag} for the $^{112}\text{Sn} + ^{112}\text{Sn}$ reactions (left panel) and $^{124}\text{Sn} + ^{124}\text{Sn}$ reactions (right panel) at the incident beam energy of 120 MeV/u with and without the HMT in semiperipheral collision. By the way, to show more clearly the isospin effects of produced isobars, we analyze the average neutron to proton ratio $\langle N/Z \rangle$ of produced isobars, which is defined as [54]

$$\langle N/Z \rangle = \frac{\sum Y(^A X_Z) (A - Z)}{Z \sum Y(^A X_Z)}, \quad (13)$$

where $\sum Y(^A X_Z)$ stands for the yield of the isobar ${}^A X_Z$ of the nuclear mass number A , the summation is over all different isobars. It is obvious that the A_{frag} distribution of average neutron to proton ratio $\langle N/Z \rangle$ is sensitive to the HMT especially for heavier fragments from Fig. 6. Moreover, we can see that $\langle N/Z \rangle$ with the HMT decreases more sharply than that without the HMT, especially for heavier isobars. This is understandable since the HMT causes de-excitation of remnants easily and usually

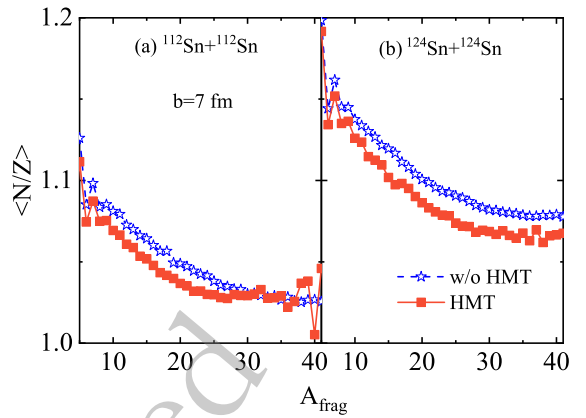


Fig. 6. (Color online) Effects of the HMT on the average neutron to proton ratio $\langle N/Z \rangle$ as a function of charge number A_{frag} in the Sn+Sn reactions at 120 MeV/u with different reaction systems.

more neutrons are emitted for neutron-rich system. Thus, the neutron-rich $^{124}\text{Sn} + ^{124}\text{Sn}$ reaction system is more sensitive to the HMT than the $^{112}\text{Sn} + ^{112}\text{Sn}$ reaction system in the A_{frag} distribution of $\langle N/Z \rangle$.

IV. CONCLUSIONS

In this work, the effects of nucleon-nucleon SRCs lead to the HMT are studied in isotopic nuclear reactions at $E_{beam} = 120$ MeV/u using the LQMD transport model. The HMT is incorporated into the initialization of nucleons of the isotopes of ^{112}Sn and ^{124}Sn in phase space. The analysis of single and double ratios of gas phase neutron and proton spectra shows that HMT affects single ratios but not double ratios in 120 MeV/u $^{112}\text{Sn} + ^{112}\text{Sn}$ and $^{124}\text{Sn} + ^{124}\text{Sn}$ reactions. Therefore, the double ratios can serve as a good experimental observable for other isospin effects. The ratio of triton-to- ${}^3\text{He}$, like the single ratios of gas-phase neutrons and protons, is influenced by the HMT, with its effects being more pronounced in neutron-rich reaction systems. The single ratios with the HMT are consistent with the experimental data, but the double ratios whether with or without the HMT can fit better to the experimental data. Finally, the isospin-dependent HMT significantly alters the fragment multiplicity distribution and the average neutron-to-proton ratio of produced isobars. Interestingly, the average neutron-to-proton ratio of heavier isobars influenced by HMT is also more pronounced in neutron-rich systems. The production of heavier fragments mainly originates from the de-excitation of remnants, which is influenced by the HMT. This differs from the production mechanism of light clusters.

References

- [1] H. A. Bethe, Ann. Rev. Nucl. Part. Sci. **21**, 93 (1971)
- [2] A. Rios, A. Polls, and W. H. Dickhoff, Phys. Rev. C **79**, 064308 (2009)
- [3] P. Yin, J. Y. Li, P. Wang *et al.*, Phys. Rev. C **87**, 014314 (2013)
- [4] C. C. de. Atti, Phys. Rep. **590**, 1 (2015)
- [5] O. Hen, G. A. Miller, E. Piasetzky, L. B. Weinstein, Rev. Mod. Phys. **89**, 045002 (2017)
- [6] J.J. Kelly, Adv. Nucl. Phys. **23**, 75 (1996)
- [7] J. Aclander *et al.*, Phys. Lett. B **453**, 211 (1999)
- [8] L. Lapikas, J. Wesseling and R. B. Wiringa, Phys. Rev. Lett. **82**, 4404 (1999)
- [9] A. Tang *et al.*, Phys. Rev. Lett. **90**, 042301 (2003)
- [10] E. Piasetzky, M. Sargsian, L. Frankfurt *et al.*, Phys. Rev. Lett. **97**, 162504 (2006)
- [11] I. Korover *et al.*, Phys. Rev. Lett. **113**, 022501 (2014)
- [12] R. A. Niyazov *et al.*, Phys. Rev. Lett. **92**, 052303 (2004)
- [13] F. Benmokhtar *et al.*, Phys. Rev. Lett. **94**, 082305 (2005)
- [14] K. S. Egiyan *et al.*, Phys. Rev. Lett. **96**, 082501 (2006)
- [15] R. Shneor *et al.*, Phys. Rev. Lett. **99**, 072501 (2007)
- [16] M. Duer *et al.*, Nature **560**, 617 (2018)
- [17] H. Baghdasaryan *et al.* (CLAS Collaboration), Phys. Rev. Lett. **105**, 222501 (2010)
- [18] N. Fomin *et al.*, Phys. Rev. Lett. **108**, 092502 (2012)
- [19] M. Duer *et al.* (CLAS Collaboration), Phys. Rev. Lett. **122**, 172502 (2019)
- [20] Q. Meng, Z. Y. Liu and C. Xu, Phys. Rev. C **108**, 014001 (2023)
- [21] Y. H. Qin *et al.*, Phys. Lett. B **850**, 138514 (2024)
- [22] S. Fantoni and V. R. Pandharipande, Nucl. Phys. A **427**, 473 (1984)
- [23] S. C. Pieper, R. B. Wiringa, and V. R. Pandharipande, Phys. Rev. C **46**, 1741 (1992)
- [24] C. C. de. Atti, S. Simula, Phys. Rev. C **53**, 1689 (1996)
- [25] K. Sh. Egiyan *et al.*, Phys. Rev. C **68**, 014313 (2003)
- [26] R. Subedi *et al.*, Science **320**, 1476 (2008)
- [27] O. Hen *et al.*, Science **346**, 614 (2014)
- [28] S. Li *et al.*, Nature **41**, 609 (2022)
- [29] K. Xiao, P. C. Li, Y. J. Wang *et al.*, Nucl. Sci. Tech. **34**, 62 (2023)
- [30] F. Y. Wang, J. P. Yang, X. Chen *et al.*, Nucl. Sci. Tech. **34**, 94 (2023)
- [31] S. N. Wei, Z. Q. Feng, Nucl. Sci. Tech. **35**, 15 (2024)
- [32] M. Q. Ding, D. Q. Fang, Y. G. Ma, Nucl. Sci. Tech. **35**, 211 (2024)
- [33] F. Zhang, Chin. Phys. Lett. **33**, 012501 (2016)
- [34] F. Zhang and G. C. Yong, Eur. Phys. J. A **52**, 350 (2016)
- [35] Z. X. Yang, X. H. Fan, G. C. Yong and W. Zuo, Phys. Rev. C **98**, 014623 (2018)
- [36] J. Y. Liu, Y. F. Yang, W. Zuo *et al.*, Phys. Rev. C **63**, 054612 (2001)
- [37] Z. Q. Feng, Phys. Rev. C **94**, 064601 (2016)
- [38] F. S. Zhang, L. W. Chen, Z. Y. Ming, and Z. Y. Zhu, Phys. Rev. C **60**, 064604 (1999)
- [39] J. Aichelin, Phys. Rep. **202**, 233 (1991)
- [40] Z. Q. Feng and G. M. Jin, Phys. Rev. C **82**, 044615 (2010)
- [41] J. Chen, Z. Q. Feng and J. S. Wang, Nucl. Sci. Tech. **27**, 73 (2016)
- [42] Z. Q. Feng, Phys. Rev. C **84**, 024610 (2011)
- [43] Z. Q. Feng, Phys. Rev. C **85**, 014604 (2012)
- [44] Z. Q. Feng, Phys. Rev. C **94**, 014609 (2016)
- [45] Y. F. Guo, P. H. Chen, F. Niu *et al.*, Chin. Phys. C **42**, 124106 (2018)
- [46] C. W. Ma, Y. J. Duan, Y. F. Guo *et al.*, Nucl. Sci. Tech. **35**, 99 (2024)
- [47] Z. Q. Feng, Phys. Rev. C **87**, 064605 (2013)
- [48] G. C. Yong, Phys. Lett. B **765**, 104 (2017)
- [49] G. C. Yong, Phys. Rev. C **93**, 044610 (2016)
- [50] O. Hen, B. A. Li, W. J. Guo *et al.*, Phys. Rev. C **91**, 025803 (2015)
- [51] G. C. Yong and B. A. Li, Phys. Rev. C **96**, 064614 (2017)
- [52] P. Morfouace *et al.*, Phys. Lett. B **799**, 135045 (2019)
- [53] D. D. S. Coupland *et al.*, Phys. Rev. C **94**, 011601(R) (2016)
- [54] D. V. Shetty *et al.*, Phys. Rev. C **68**, 054605 (2003)